# Characterization of coenzyme binding and selectivity determinants in Mycobacterium tuberculosis FprA: analysis of Arg199 and Arg200 mutants at the NADP(H) 2'-phosphate binding site

Muna Sabri, Adrian John Dunford, Kirsty Jane Mclean, Rajasekhar Neeli, Ns Scrutton, David Leys, Andrew W Munro

# Characterization of coenzyme binding and selectivity determinants in *Mycobacterium tuberculosis* flavoprotein reductase A

## Analysis of Arg199 and Arg200 mutants at the NADP(H) 2'-phosphate binding site.

**Muna Sabri, Adrian J. Dunford, Kirsty J. McLean, Rajasekhar Neeli, Nigel S. Scrutton, David Leys and Andrew W. Munro***

[1]Manchester Interdisciplinary Biocentre, The University of Manchester, Faculty of Life Sciences, 131 Princess Street, Manchester M1 7DN, UK.

*Author for correspondence: Prof. Andrew W. Munro. Phone; 0044 161 306 5151; Fax, 0044 161 306 8918. E-mail: Andrew.Munro@Manchester.ac.uk

**Running title**: Coenzyme selectivity determinants in *M. tuberculosis* FprA

## SYNOPSIS

*Mycobacterium tuberculosis* flavoprotein reductase A (FprA) is a NAD(P)H- and FAD-binding reductase that is structurally/evolutionarily related to adrenodoxin reductase. Structural analysis implicates arginines 199 and 200 in interactions with the NADP(H) 2'-phosphate group. R199A, R200A and R199A/R200A mutants were characterized to explore the roles of these basic residues. All mutations abolished neutral FAD semiquinone stabilization in NADPH-reduced enzyme, owing to weakened NADPH affinity. Instead, FAD hydroquinone was formed in all mutants, and each displayed substantially enhanced auto-oxidation rates (20-40 fold) compared to NADPH-reduced wild-type FprA. Steady-state ferricyanide reduction studies revealed diminished NADPH affinity (higher $K_m$ values), but lower NADH $K_m$ values. Despite a lowered $k_{cat}$, the R199A/R200A mutant exhibited a 200-fold coenzyme specificity switch towards NADH, although substrate inhibition was observed at high NADH concentrations ($K_i$ = 250 μM). Stopped-flow FAD reduction studies confirmed substantially increased NADPH $K_d$ values, although the limiting flavin reduction rate constant was similar in all mutants. The R199A mutation abolished electron transfer between hydroquinone FprA and $NADP^+$, while this reaction progressed (*via* a $FADH_2$-$NADP^+$ charge-transfer intermediate) for R200A FprA, albeit more slowly ($k_{lim}$ = 58.1 $s^{-1}$ *versus* >300 $s^{-1}$) than in wild-type. All mutations caused positive shifts in FAD potential (~40-65 mV). Binding of a NADPH analogue (tetrahydro-NADP) induced negative shifts in potential (~30-40 mV) only for variants with the R200A mutation, indicating distinctive effects of Arg199/Arg200 on coenzyme binding mode and FAD potential. Collectively, these data reveal important roles for the phylogenetically conserved arginines in controlling FprA FAD environment, thermodynamics, coenzyme selectivity and reactivity.

**Keywords**: *Mycobacterium tuberculosis*, flavoprotein reductase A, adrenodoxin reductase, coenzyme binding, electron transfer, enzyme mechanism.

**Abbreviations**: AdR – adrenodoxin reductase; FprA – flavoprotein reductase A from *Mycobacterium tuberculosis*; $H_4NADP$ – tetrahydro NADP; HQ – hydroquinone; Mtb – *Mycobacterium tuberculosis*; PDA – photodiode array; SQ – semiquinone; WT – wild-type.

## INTRODUCTION

*Mycobacterium tuberculosis* (Mtb), the causative agent of tuberculosis (TB), is once again established as a leading cause of human mortality worldwide [1]. Its re-emergence has been linked to its opportunistic infection of HIV-infected individuals, and to the increasing ineffectiveness of the most widely used antitubercular drugs (including antibiotics such as rifampicin, isoniazid and ethionamide) [2]. Antibiotic resistance, in turn, is associated with patients failing to complete courses of drugs and as a consequence of mutations in target proteins that lead to diminished drug binding or their failure to activate pro-drugs (e.g. the common S315T mutation that leads to diminished efficiency of the Mtb catalase-peroxidase enzyme KatG in its activation of isoniazid to a toxic radical form) [3]. The World Health Organization has recognized the global threat to human health posed by multidrug resistant strains of Mtb, and has highlighted the desperate requirement for novel therapies to combat antibiotic resistant strains [4].

The genome sequence of Mtb (strain H37Rv) determined by Cole and co-workers revealed several unusual features and provided important information in the search for new antitubercular therapies [5]. In particular, a large cohort of enzymes involved in the complex lipid metabolism of Mtb was revealed, and an unexpectedly large number (20) of cytochrome P450-encoding (CYP) genes were identified in the genome [6]. The P450s are mono-oxygenase enzymes involved in a diverse range of catalytic processes in organisms from all of the domains of life. The presence of so many P450s in Mtb (the Mtb *CYP* gene "density" is ~240-fold greater than in the human genome) indicates important roles in physiology and infectivity [6]. In particular, the identification of the first bacterial sterol demethylase P450 in Mtb (CYP51B1) highlighted the possibility that azole drugs might be effective as antituberculars [7,8]. Azoles such as fluconazole, clotrimazole and econazole are widely used antifungal therapies that act by inhibiting the sterol demethylase CYP51 and so prevent synthesis of ergosterol, an important determinant of fungal membrane fluidity [9]. Recent studies of the effects of azole drugs on various mycobacteria and other actinobacteria showed that a number of these antibiotics were inhibitory to growth, and it was demonstrated that econazole was effective in clearing Mtb infection from the spleens of infected mice [6,10,11].

The Mtb P450 enzymes require redox partner systems for electron delivery to the P450s to enable substrate oxidation. Typical bacterial P450 redox systems involve NAD(P)H-dependent, FAD-binding ferredoxin/flavodoxin reductase (FDR) enzymes, and ferredoxin (FD) proteins that mediate single electron transport to the P450s [12]. In Mtb, there are a number of ferredoxins identifiable in the genome sequence, and the 3Fe-4S ferredoxin Fdx (product of gene *Rv0763c*) is encoded adjacent to the CYP51B1 enzyme (*Rv0764c*) in the Mtb H37Rv genome [8,13]. An obvious candidate FDR-type protein is FprA (flavoprotein reductase A), which has significant amino acid sequence and protein structural identity with mammalian mitochondrial adrenodoxin reductase (AdR) enzymes that participate in P450 redox systems involved in steroidogenesis [14-17]. In previous studies, the expression and purification of FprA was reported, and the kinetic and thermodynamic features of the wild-type (WT) enzyme were established [14,15]. FprA (along with the Mtb Fdx ferredoxin) was shown to support an electron transfer system that delivered electrons from NADPH to the Mtb P450 CYP51B1 and to the structurally resolved CYP121 [8,13,18]. FprA was shown to be reduced to the (neutral) blue semiquinone (SQ) form by NADPH, but fully to the hydroquinone (HQ) form by NADH, despite the identical redox potentials of these coenzymes [14,19]. This finding revealed important differences in the nature of the interactions between FprA and NADPH/NADH, and pointed towards interactions between NADP(H) and reduced WT FprA that resulted in stabilization of the SQ form, and which did not occur with NAD(H) [15].

To explore further this phenomenon and to rationalise coenzyme selectivity and its molecular basis in FprA, we investigated the effects of mutating residues predicted to be important in interactions with the 2'-phosphate group of NADP(H); the sole difference between this coenzyme and NAD(H). Examination of the atomic structure of Mtb FprA revealed that two arginine residues (Arg199 and Arg200) were likely to make favourable interactions with the 2'-phosphate group of NADP(H), and suggested that these residues could be critical in pyridine nucleotide coenzyme selectivity and in controlling the distinctive reductive processes observed with NADPH and NADH in the WT enzyme (Figure 1) [14,15]. In this paper we report the detailed characterization of the R199A, R200A and R199A/R200A FprA mutants, revealing important

roles for these basic residues in the regulation of coenzyme selectivity, flavin thermodynamics and catalytic efficiency of this important *M. tuberculosis* enzyme.

## EXPERIMENTAL

**Construction of FprA mutants**. Mutagenesis of the *fprA* gene to create R199A, R200A and R199A/R200A mutants was done with the Stratagene QuikChange kit, using plasmid pKM3b (encoding WT FprA [15]) as the template and *Pfu* Turbo® DNA polymerase. Oligonucleotide primers used and the mutagenesis procedures employed are described in full in the *Supplementary Data* section. All clones isolated were completely sequenced to ensure the presence of desired mutations and the absence of adventitious mutations.

**Purification of WT FprA and FprA mutants**. WT FprA and mutant proteins were produced in the T7 RNA polymerase lysogen strain HMS174 (DE3) (Novagen). HMS174 (DE3)/pFprA R199A, R200A and R199A/R200A transformants (typically 10-30 litres) were grown at 37 °C with vigorous agitation (220 rpm) until mid-logarithmic growth phase ($OD_{600}$ ~0.7) in either YT or Terrific Broth media [20]. Culture temperature was then decreased to 25 °C, and expression of WT and mutant *fprA* genes was induced by addition of IPTG (1 mM) once the $OD_{600}$ = 1.0. Culture growth was continued for 16–20 h. Cells (typically 30–50 g wet weight) were harvested and disrupted, and WT FprA protein was purified to homogeneity using methods established previously for WT and Trp359 mutants of FprA [15,19]. Purification methods for the FprA mutants are described in more detail in the *Supplementary Data* section. Subsequent enzyme characterization was performed in 10 mM sodium phosphate, pH 7.5 (Buffer A), unless otherwise stated. Purity of FprA proteins was assessed by spectral analysis (ratio of flavin-specific absorption [$A_{452}$] to protein specific absorption [$A_{274}$]) and by SDS/PAGE of protein samples at different stages of purification. FprA concentration was determined using the oxidised enzyme coefficient: $\varepsilon_{452}$ =10.6 $mM^{-1}$ $cm^{-1}$ [15].

**Steady-state and stopped-flow kinetic analysis of mutant FprA enzymes**. WT and mutant FprA-catalysed reduction of potassium ferricyanide was analysed by steady-state kinetic measurements using both NADH and NADPH as electron donors. NAD(P)(H) coenzymes were from Melford (Ipswich, UK). Kinetic parameters ($K_m$, $k_{cat}$) for ferricyanide reduction were determined in buffer A and also in 50 mM Tris.HCl (pH 7.5) at 30 °C. Enzyme concentration was typically 50-100 nM. Ferricyanide concentration was maintained at 1.5 mM in reactions where NAD(P)H concentrations were varied (typically up to 1 mM coenzyme) to establish $K_m$ values for the coenzymes. In reactions where the concentration of the electron acceptor (ferricyanide) was varied, NAD(P)H concentrations were maintained at near-saturating concentrations established from the preceding assays and confirmed in this work (200 µM for NADPH) [15]. Ferricyanide reduction was determined at 420 nm ($\Delta\varepsilon_{420}$ = 1020 $M^{-1}$ $cm^{-1}$). All measurements were in triplicate at each substrate concentration and all data points varied by <5 % from the mean. The observed rate *versus* substrate concentration data were fitted to the Michaelis-Menten function to establish the $k_{cat}$ and $K_m$ parameters, except in the case of data for NADH-dependent reduction of ferricyanide in the R199A/R200A double mutant where substrate inhibition was observed. In this case, data were fitted instead to a substrate inhibition equation (Equation 1) as follows; where $k_{obs}$ is the observed rate at substrate concentration $S$, $K_i$ is the dissociation constant for the substrate acting as inhibitor, and $K_m$ and $k_{cat}$ are the Michaelis-Menten parameters.

$$k_{obs} = \frac{k_{cat}[S]}{K_m + [S](1 + ([S]/K_i))} \qquad \textbf{Equation 1}$$

Stopped-flow studies of the reductive half reaction of FprA mutants R199A, R200A and the double mutant (R199/R200A) were performed using an Applied Photophysics SX.18 MVR stopped-flow spectrophotometer contained within a glove box (Belle Technology, Portesham, UK) to maintain anaerobic

conditions (<5 ppm oxygen). Flavin reduction by NADH/NADPH (up to 2.5 mM) was monitored by bleaching of the flavin in single wavelength mode at 452 nm (at the FprA flavin absorption peak) with enzyme typically at 5-10 μM. Flavin reduction rates for mutant proteins were measured at 30 °C. All measurements were carried out in buffer A. All buffers were deoxygenated by evacuation and extensive bubbling with oxygen-free nitrogen. Prior to stopped-flow studies, protein samples were fully oxidised by treatment with potassium ferricyanide; and excess ferricyanide was removed by rapid gel filtration in the glove box (Pharmacia PD-10 column). Absorption transients from stopped-flow experiments were fitted to appropriate exponential functions using Spectrakinetics software (Applied Photophysics). Observed flavin reduction rates for FprA mutants reduced by NAD(P)H ($k_{obs}$) showed a hyperbolic dependence on coenzyme concentration. Rate *versus* coenzyme concentration data were fitted to Equation 2 [21] to determine the apparent enzyme-coenzyme dissociation constant, $K_d$, and limiting rate of electron transfer to the FAD ($k_{lim}$). Values reported are averages of at least three separate determinations at each coenzyme concentration.

$$k_{obs} = \frac{k_{lim}[S]}{K_d + [S]} \qquad \textbf{Equation 2}$$

Stopped-flow, multiple-wavelength scanning absorption studies were also done using a photodiode array (PDA) detector and X-SCAN software (Applied Photophysics). Reactions were typically performed using an enzyme concentration of 40 μM in buffer A (20 μM in the final mixture) and over timescales up to 5 seconds after the initial mixing event, with the first spectrum generally recorded at 1.3 milliseconds after mixing. NADH and NADPH (at concentrations up to 200 μM in the final mixture) were mixed with oxidised enzymes. Recorded spectra were then analysed globally using the Applied Photophysics ProKin software package, to investigate the formation of any distinct intermediate spectral forms and to define their rates of formation.

The oxidative half reaction was also investigated by the ability of sodium dithionite-reduced FprA mutants to pass electrons to $NAD^+$ and $NADP^+$. R199A, R200A and the double mutant were made anaerobic and reduced by addition of a small excess of sodium dithionite in a glove box. The enzymes were separated from reductant by gel filtration using a BioRad Econo-Pac 10DG desalting column in the anaerobic box, pre-equilibrated with degassed buffer. The reduced enzyme was diluted to 20-40 μM in 50 mM sodium phosphate (pH 7.5) containing 5 % glycerol, and then mixed with $NAD^+$ or $NADP^+$ (up to a final concentration of 400 μM, i.e. 10-fold excess over the enzyme in the mixture) in the stopped-flow apparatus. Measurements of the rate of electron transfer from FprA to the coenzyme were made both in single wavelength mode (452 nm) and using a PDA as above. Data analysis was as described above for the reductive half-reaction.

Aerobic flavin reoxidation in FprA and its mutants (20 μM) was monitored at 30 ºC in 100 mM potassium phosphate, pH 7.5, following addition of a stoichiometric amount of NAD(P)H. Reoxidation was measured through analysis of the rate of recovery of flavin absorption at 452 nm, and by fitting a single exponential function to the absorption *versus* time data using Origin 7.5 software (OriginLab, Northampton MA).

**Spectroscopic analysis**. All UV-visible absorption spectra and steady-state assays for FprA enzymes were recorded using a Cary UV-50 Bio UV-visible scanning spectrophotometer (Varian UK). Samples were suspended in buffer A for spectral analysis. Samples (typically ~40-50 μM) were analysed using a 1 cm pathlength quartz cuvette. Circular dichroism (CD) measurements were performed at 20 °C using a JASCO J700 spectrapolarimeter with samples prepared in buffer A. Far-UV CD spectra were recorded from 190-260 nm in a quartz cell of 0.05 cm path length and with a scan rate of 10 nm/min. All spectra were recorded in triplicate and averaged. Protein concentrations used were 10.5 μM for far-UV CD measurements.

**Analysis of flavin redox potentials**. Potentiometric redox titrations to determine the midpoint reduction potentials of the FAD cofactor in the R199A, R200A and R199A/R200A FprA mutants were performed in a Belle Technology glove-box under a nitrogen atmosphere, as described previously for WT and Trp359 mutants of FprA and for related enzymes [15,19,22]. All solutions were degassed under vacuum with nitrogen. Oxygen levels were always maintained at less than 2 ppm. 100 mM potassium phosphate, pH 7.0, containing 10 % v/v glycerol (titration buffer) was used in all potentiometric titrations. FprA proteins (typically 40–80 μM in ~5 ml titration buffer) were titrated electrochemically according to the method of Dutton [23]. Details of mediators and the electrode system used are in the *Supplementary Data* section. Data manipulation and analysis were performed using Origin 7.5 software. For analysis of flavin midpoint potentials, absorbance data at 452 nm were plotted against applied potential and the data were fitted using a 2-electron Nernst equation to define the midpoint reduction potential for the 2-electron transition (i.e. the FAD oxidised/HQ redox couples), as described previously [23-25].

## RESULTS

**Generation, expression and purification of FprA mutants.** An examination of the crystal structure of Mtb FprA revealed the likely involvement of two arginine residues (Arg199 and Arg200) in interactions with the 2'-phosphate group of NADP(H) [14]. An analysis of the amino acid sequences of related FprA enzymes in other mycobacteria, AdR enzymes from various eukaryotes and other homologous enzymes revealed that these arginine residues were implicitly conserved, and thus likely to play important roles in coenzyme recognition/selectivity in all these enzymes (see *Supplementary Data* Figure S1). To investigate roles of these residues, the three Mtb FprA mutants: R199A, R200A and the R199A/R200A double mutant were generated by site-directed mutagenesis, verified by restriction digestion and DNA sequencing, and the encoded proteins isolated as described in the *Experimental* and *Supplementary Data* sections. Levels of *fprA* expression in the R199A and R200A mutant transformants was diminished compared to WT *fprA*, but a more extensive culture period (~20 hr rather than 12 hr for WT *fprA*) resulted in production of comparable amounts of proteins (~2 mg/litre culture). However, expression levels were further reduced for the R199A/R200A double mutant and only ~0.5 mg protein/litre culture were recovered. Thus, larger scale protein production cultures were typically grown for the double mutant FprA transformant than for WT and point mutant transformants. The R199A and R200A and double mutant FprA proteins were purified using the same procedures as for WT FprA (chromatographic separations on phenyl Sepharose and Q-Sepharose resins) until the stage of affinity chromatography (on 2', 5'-ADP agarose) that was used successfully only for purification of WT FprA [15,19]. The mutant proteins did not bind well to this resin, consistent with effects on the NADP(H) affinity caused by R199A and R200A mutations. Instead, a new chromatographic step using affinity for hydroxyapatite (see *Experimental* and *Supplementary Data* sections) was used to further purify the mutant proteins. WT and mutant FprA proteins were subjected to a final purification step by gel filtration on Sephacryl S-200 resin. The purified mutant proteins exhibited a final protein/flavin (FAD) absorbance ratio ($A_{274}/A_{452}$) of <7, consistent with that for WT FprA and indicative of pure holoprotein in each case.

**Electronic absorption properties for oxidised and mutant FprA proteins.** The electronic absorption properties of the R199A, R200A and R199A/R200A proteins were determined for the oxidised enzymes, and for the enzymes reduced with either NADPH, NADH or sodium dithionite. In their oxidised forms, the UV-visible absorption spectra were not significantly perturbed from those for the WT FprA. All had the typical flavin absorption bands at 452 nm and at 379 ± 1 nm, and exhibited a pronounced shoulder on the longer wavelength absorption band at 476 ± 1 nm (Figure 2). Circular dichroism (CD) studies of the mutants in the far UV region (190-260 nm) revealed no significant changes compared to WT FprA and thus indicated that the secondary structural properties of FprA were not disrupted by the mutations (not shown). Thus, these mutations, which are located outside the immediate environment of the isoalloxazine ring, do not appear to grossly affect the electronic structure or environment of this redox active portion of the oxidised FAD cofactor, or to affect protein folding. However, there were clear differences in the optical

absorption spectra between WT and all of the mutant FprA proteins in their NADPH-reduced forms. As observed previously, reduction with sodium dithionite ($E_m$ = -420 mV) and with NADH ($E_m$ = -320 mV, 100 μM) resulted in the conversion of WT FprA from its quinone (oxidised state) to its 2-electron reduced HQ form. However, reduction with NADPH ($E_m$ = -320 mV, 100 μM) resulted in the production of a partially reduced WT FprA with a substantial component of 1-electron reduced blue SQ. By contrast, reduction of the R199A, R200A and double mutant FprA proteins with dithionite, NADH or NADPH resulted in the near-complete reduction of the FAD to the HQ form in all cases. Only for the R200A mutant was there a very small proportion of SQ remaining following reduction by NADPH (Figure 2). The stabilization of the SQ form of WT FprA was previously assigned to the tight binding of NADPH to both the oxidised and HQ forms of FprA, followed by electronic comproportionation between pairs of such molecules to form two molecules of NADPH-bound SQ FprA [15]. Thus, the destabilization of the FAD SQ in the FprA mutants (and particularly in those carrying the R199A mutation) was likely due to diminished affinity for NADP(H) and/or to altered thermodynamic properties of the flavin. To probe further the effects of mutations on FprA and coenzyme selectivity/electron transfer, we examined the kinetic properties of WT and FprA using steady-state and stopped-flow approaches.

**Steady-state kinetic analysis of WT and mutant FprA enzymes.** In previous studies, it was shown that ferricyanide was a good substrate for reduction by WT FprA using both NADPH and NADH coenzymes as the electron donors. The WT FprA $K_m$ value for NADPH was substantially lower than that for NADH [15,26]. To determine the influence of the R199A, R200A and R199A/R200A mutations on the catalytic efficiency with the different coenzymes in steady-state turnover, analysis of the reduction of ferricyanide was done both to determine (i) the $k_{cat}$ and $K_m$ parameters for the coenzymes (with ferricyanide at a near-saturating concentration of 1.5 mM) and (ii) the same parameters for ferricyanide (with NADPH at 200 μM; a concentration established as near-saturating from the initial set of assays at fixed ferricyanide concentration). Data collected using buffer A are presented in Table 1. A parallel data set was also collected in 50 mM Tris.HCl buffer (pH 7.5), and showed little relevant variations from the data presented in Table 1. The data reveal that the $k_{cat}$ value for WT FprA with NADH as reducing coenzyme (2720 ± 90 $min^{-1}$) is slightly greater than with NADPH (2070 ± 100 $min^{-1}$), possibly reflecting higher affinity for $NADP^+$ product in the WT enzyme. Consistent with this conclusion, the $k_{cat}$ values for the R199A and R200A mutants (with NADPH as electron donor) were elevated towards those values observed for WT and for these two point mutant FprA enzymes with NADH as electron donor (e.g. R199A $k_{cat}$ [NADPH] = 2880 ± 130 $min^{-1}$; $k_{cat}$ [NADH] = 2960 ± 70 $min^{-1}$). While the $K_m$ values for ferricyanide were not considerably perturbed in the point mutants (5.9 μM [WT]; 4.0 μM [R199A]; 6.7 μM [R200A]), the $K_m$ values for NADPH were increased 6.3-fold (R199A) and 3.2-fold (R200A), while those for NADH were decreased 2.7-fold (R199A) and 5.3-fold (R200A). The net effects were a 4.5-fold (R199A) and 2.6-fold (R200A) decrease in the specificity constant ($k_{cat}/K_m$ ratio) with NADPH (compared to WT FprA); but a 2.9-fold (R199A) and 5.3-fold (R200A) increase in specificity constant with NADH (compared to WT FprA). Collectively, the catalytic effects mediated by the point mutations result in an approximately 13.3-fold switch in coenzyme preference from NADPH towards NADH for both the R199A and R200A mutants, as determined from the ratio of the specificity constants with the respective coenzymes (Table 1).

For the double mutant (R199A/R200A) FprA, there are distinctive effects on catalysis of ferricyanide reduction compared to those mediated by the individual mutations. The $k_{cat}$ value is decreased >6-fold with NADPH as electron donor (302 ± 23 $min^{-1}$), and the $K_m$ value for this coenzyme (16.7 ± 4.7 μM) is also 4.4-fold greater than for WT FprA, leading to a 30-fold decrease in the specificity constant. With NADH as electron donor, there is clearly substrate inhibition observed regardless of buffer system used. Data fitting using Equation 1 provided parameters of $k_{cat}$ = 830 ± 38 $min^{-1}$, $K_m$ = 18.8 ± 5.3 μM and $K_i$ = 250 ± 52 μM for the reactions performed in buffer A. The switch in specificity for this mutant (again from ratio of specificity constants for NADH and NADPH) is 200-fold towards NADH, largely as a result of the much lower $K_m$ value for NADH compared to WT FprA (18.8 *versus* 427 μM) (Table 1). The substrate inhibition effect is only seen for the double mutant with NADH and likely reflects distinctive

binding modes (productive and non-productive) that are accessible for this coenzyme following the removal of both bulky basic residues.

**Transient kinetic studies of FAD reduction in WT and mutant FprA enzymes.** Previous studies of the transient kinetics of reduction of WT FprA indicated a hyperbolic dependence of FAD reduction rate on NADH concentration (limiting electron transfer rate, $k_{lim}$, = 25.4 ± 0.7 $s^{-1}$; $K_d$ = 42.9 ± 4.6 μM), but a lack of dependence of FAD reduction rate on NADPH concentration under *pseudo* first order conditions for the coenzyme ($k_{lim}$ = 20 ± 2 $s^{-1}$) [15]. For each of the R199A, R200A and double mutants, FAD reduction transients fitted well to a single exponential function with both NADH and NADPH as reducing coenzymes. With NADH (in all cases) the dependence of FAD reduction rate on coenzyme concentration remained hyperbolic, with the kinetic parameters for the R199A and R200A mutants being broadly similar to that for WT FprA ($k_{lim}$ = 25.7 ± 0.9 $s^{-1}$; $K_d$ = 54.0 ± 9.4 μM [R199A], and $k_{lim}$ = 24.9 ± 1.0 $s^{-1}$; $K_d$ = 32.1 ± 7.2 μM [R200A]). The double mutant had a similar $k_{lim}$ (26.7 ± 1.4 $s^{-1}$) and a further small increase in the $K_d$ value (64.4 ± 13.9 μM) (Table 2). For reduction with NADPH, it was found that reaction transients remained monophasic in all mutants, but that the dependence of FAD reduction rate on NADPH concentration was now also hyperbolic. This again indicated a decrease in affinity for NADPH, consistent with steady-state data and with the expected roles of Arg199/Arg200 in binding the coenzyme 2'-phosphate group. The kinetic parameters determined were $k_{lim}$ = 29.0 ± 0.7 $s^{-1}$; $K_d$ = 28.3 ± 4.3 μM (R199A); $k_{lim}$ = 27.5 ± 0.5 $s^{-1}$; $K_d$ = 42.6 ± 5.8 μM (R200A); and $k_{lim}$ = 22.2 ± 0.5 $s^{-1}$; $K_d$ = 88.6 ± 7.7 μM (double mutant). Thus, the $k_{lim}$ values with NADPH were similar to those for WT FprA, but apparent affinity for NADPH was diminished in the single mutants, and the effect was compounded in the double mutant. Exemplary data sets describing the relationship between FAD reduction rate and coenzyme concentration are shown for the NADPH-dependent reduction of the R200A variant and the R199A/R200A double mutant in Figure 3 and Figure S2 in the *Supplementary Data*, respectively. The insets show examples of fitted flavin reduction transients from the respective data sets. Photodiode array stopped-flow spectroscopy studies of the NAD(P)H-dependent reduction of the FprA mutants were done to follow spectral development during flavin reduction. These studies demonstrated reductive transitions between oxidised (quinone) and 2-electron reduced (HQ) forms of the FAD cofactor, and with no evidence for any formation of blue SQ species seen at equilibrium in the reaction between WT FprA and NADPH [15]. These data were thus consistent with equilibrium reduction spectra shown in Figure 2 and further confirmed the destabilization of the blue SQ species induced by both the R199A and R200A mutations in FprA. Figure 4 (panels A and B) shows exemplary PDA data sets for the NADPH-dependent reduction of the R199A and R200A mutants, respectively.

**Analysis of the oxidative reactions of reduced FprA mutants.** Previous stopped-flow studies of the reactions of WT FprA with NAD(P)H demonstrated that there was negligible reoxidation of the dithionite-reduced (HQ) enzyme with $NAD^+$ as the oxidant (under anaerobic conditions), but that there was rapid partial reoxidation with $NADP^+$ as the oxidant, leading to a final species with spectral properties similar to that obtained for the reductive reaction between oxidised FprA and NADPH at a similar concentration (i.e. with blue SQ FAD formed) [15]. In view of the perturbations to the NAD(P)H binding site induced by the R199A and R200A mutations (alone and in combination), we examined the oxidative reaction of the dithionite-reduced mutants with $NAD(P)^+$ on a stopped-flow time scale time scale by both PDA and single wavelength analysis to monitor FAD electron transfer to the coenzyme under anaerobic conditions. It was found that incubation of dithionite-reduced enzymes in buffer A resulted in some enzyme precipitation over time, and for this reason oxidative reactions were done in 50 mM sodium phosphate (pH 7.5) containing 5 % glycerol to aid protein stability. As with WT FprA, and even at the highest concentrations of $NAD^+$ used (200 μM, a 10-fold excess over the enzyme concentration), there was negligible oxidation of the R199A, R200A and R199A/R200A mutants (< 3 %) over periods of up to 200 seconds following the mixing event. With $NADP^+$ as the oxidizing coenzyme, substantial reoxidation was observed for the R200A mutant, but the R199A and R199A/R200A mutants showed a far lower level of reoxidation (Figure 4, panels C and D). For the R200A mutant, the enzyme reoxidises to ~40 % completion (with 200 μM $NADP^+$ as oxidant)

within 0.5 s following the stopped-flow mixing event, and there is clear development of a long wavelength charge transfer (CT) species immediately following mixing of the R200A HQ FprA with $NADP^+$, which subsequently decays as the process of electron transfer to $NADP^+$ (forming NADPH) progresses (Figure 4D). This CT species occurs due to the reaction between the reduced FAD and the oxidised coenzyme, and is indicative of productive interaction between the coenzyme nicotinamide and FAD isoalloxazine ring in readiness for the electron transfer event. By contrast, the R199A and R199A/R200A mutants reoxidise to only ~5 % completion over 200 s, and there is no evidence of formation of a CT complex, suggesting that the R199A mutation results in disorientation of the oxidised coenzyme nicotinamide ring in the FprA active site, such that electron transfer from the FAD to $NAD(P)^+$ in the reduced (HQ) R199A and R199A/R200A mutants becomes inefficient. In single wavelength (452 nm) anaerobic stopped-flow absorption studies, the reaction of the reduced R200A FprA enzyme with $NADP^+$ (up to 500 μM) was analysed, and a hyperbolic dependence of FAD oxidation rate (determined by fitting reaction transients with a single exponential function) on coenzyme concentration was obtained, producing parameters of $k_{lim}$ = 58.1 ± 0.2 $s^{-1}$ and $K_d$ = 11.6 ± 0.2 μM. However, this rate of (partial) reoxidation of R200A $FADH_2$ to $NADP^+$ remains substantially lower than was reported previously for WT FprA (>300 $s^{-1}$) [15].

In view of the disruption of the NAD(P)H binding site induced by the R199A and R200A mutations, and in light of the altered reactivity with $NAD(P)^+$ above, we also examined the reoxidation of the reduced WT and all mutant FprA enzymes (20 μM) under aerobic conditions with molecular oxygen as the electron acceptor. Enzymes were reduced with stoichiometric NADH or NADPH, as described in the *Experimental* section. The reoxidation rate data are presented in Table 3. It is clear that with NADH as the reductant, oxidation rate for the WT FprA (1.26 ± 0.06 $min^{-1}$) is not substantially different from those of the other mutants, although the R199A variant reoxidises slightly slower than WT FprA (0.88 ± 0.03 $min^{-1}$). However, with NADPH as the reductant there is a substantial difference in oxidation rate for WT FprA compared to the situation with NADH as reductant. The NADPH-reduced WT FprA oxidises much more slowly (0.043 ± 0.004 $min^{-1}$), likely as a consequence of its higher affinity for NADP(H), which in turn enables stabilization of the blue SQ species. By contrast, each of the NADPH-reduced mutants reoxidise ~18-26 fold faster than the WT FprA (Table 3). These data emphasise the importance of the binding of NADP(H) coenzyme in the stabilization of the reduced forms of FprA, and reinforce the detrimental effects of the arginine mutations on both the affinity for NADP(H) and the resultant enhanced auto-oxidation of the mutants.

**Thermodynamic analysis of the FprA mutants.** The preceding studies of reduction potentials of WT FprA demonstrated the absence of stabilization of blue SQ during equilibrium titrations with dithionite (reductant) and ferricyanide (oxidant). Similar phenomena were observed in redox titrations of the R199A, R200A and R199A/R200A mutants, highlighting the importance of NADP(H) coenzyme binding in stabilizing the SQ form. The midpoint 2-electron reduction potential for WT FprA is -230 ± 12 mV, and this was not significantly altered (-235 ± 5 mV) when the protein was bound to a non-redox active analogue of NADPH (tetrahydro-NADP, or $H_4$NADP) [8]. FAD reduction potentials were determined for the ligand-free and $H_4$NADP-bound forms of the R199A, R200A and R199A/R200A mutants. Data are presented in Table 4. In all cases, there was negligible stabilization of SQ in the titrations. However, in all cases the FAD potentials were more positive than that for WT FprA (by ~38-65 mV), indicating a change in FAD isoalloxazine environment in all cases. For the R199A mutant, the potential was not considerably altered in the $H_4$NADP complex. However, for both the R200A and R199A/R200A mutants the FAD potential is much more negative in the $H_4$NADP complex, and in the case of the R200A mutant the potential is decreased by 41 mV and to a value identical within error to that for the WT FprA $H_4$NADP complex (Figure 5). The data demonstrate that the environment of the FprA FAD is perturbed in the arginine mutants, leading to positive changes in the FAD midpoint potential compared to WT, and that the binding of the coenzyme analogue $H_4$NADP causes negative shifts in potential, and particularly for those variants carrying the R200A mutation.

## DISCUSSION

Arginine residues corresponding to Arg199 and Arg200 are widely conserved in FprA- and AdR-like enzymes from several organisms (see *Supplementary Data* Figure S1). Analysis of the Mtb FprA atomic structure suggested that both these arginines are important to the binding of the 2'-phosphate group of NADP(H) coenzyme, while Arg199 also interacts with the adenosine moiety through π–π stacking interactions [14]. In view of the unusual ability of FprA to stabilise a blue SQ FAD only with NADPH as reductant, we created the R199A, R200A and R199A/R200A mutants and performed detailed catalytic, kinetic, spectroscopic and thermodynamic studies to investigate the roles of these residues. In previous studies, the stabilization of the neutral blue SQ form of the WT FprA FAD was assigned to the binding of NADPH to both the reduced (HQ) and oxidised forms of FprA, followed by electronic comproportionation to produce the SQ species as the predominant form [15,26]. While only minor effects were observed on secondary structure or oxidised spectra of the mutant proteins, equilibrium reduction with NADPH (or NADH) results in near complete HQ formation, suggesting that NADP(H) binding is destabilized by comparison with WT FprA. This was consistent with the finding that the arginine mutants no longer bound a NADP(H) coenzyme affinity resin, and with higher mutant $K_m$ values for NADPH (Table 1). Stopped-flow FprA FAD reduction studies also demonstrated that NADPH affinity was diminished in mutants, with $K_d$ values increasing in the order R199A<R200A<R199A/R200A (Table 2). The $K_m$ values for NADH were improved in all mutants, suggesting an important role for the Arg199 and Arg200 in discriminating against this coenzyme, and $k_{cat}/K_m$ ratios also indicated a substantial specificity switch towards NADH in the mutants (Table 1). For its role in a Mtb P450 redox system, FprA provides electrons one at a time to ferredoxin(s), which themselves are obligate one electron transfer proteins [27]. Thus, it is feasible that the NADPH-dependent stabilization of the FprA SQ is related to its preferred electron transfer mechanism in a class I P450 redox system. However, it is also clear that the oxidation of FAD in NADPH-reduced WT FprA is substantially slower (18-fold or more) than in the arginine mutants, which also points to this being a mechanism for avoiding auto-oxidation and wastage of reducing equivalents *in vivo* (Table 3).

Potentiometry showed that all mutations resulted in more positive FAD reduction potentials, indicating perturbation of the isoalloxazine environment, despite the arginines not being involved directly in bonding interactions with this redox active portion of the FAD cofactor. Binding of the redox inactive NADPH analogue $H_4$NADP to FprA variants containing the R200A mutation resulted in a negative shift in FAD midpoint potential (~30-40 mV) consistent with this mutation affecting the binding mode of $H_4$NADP such that the FAD environment is perturbed in the complex. No substantial shifts in FAD potential were noted for $H_4$NADP-bound WT or R199A FprA (Table 4) [15]. Interestingly, the oxidative reaction of HQ R200A FprA with $NADP^+$ results in transient formation of a CT species between reduced enzyme and oxidised coenzyme ($FADH_2$:$NADP^+$), followed by a rapid electron transfer reaction until an equilibrium mixture of $FADH_2$/$NADP^+$ and FAD/NADPH species is produced (Figure 4D). The observed rate of this oxidative reaction (at 200 μM $NADP^+$) is slower for R200A FprA (58.1 $s^{-1}$) than for WT FprA (>300 $s^{-1}$), but remains an efficient process. By contrast, negligible $NADP^+$-dependent oxidation occurs for the R199A or double mutant FprA enzymes, indicating that Arg199 plays a critical role in facilitating the orientation of the $NADP^+$ coenzyme and its nicotinamide to enable electron transfer in the oxidative direction. Negligible electron transfer from the $FADH_2$ species occurs to $NAD^+$ on a stopped-flow timescale for WT or any of the arginine mutants.

FprA likely plays a pivotal role in supporting the activity of several Mtb P450 enzymes. We have previously demonstrated FprA-dependent electron transport to the Mtb CYP51B1 and CYP121 P450s [8,28]. A number of Mtb P450s have been shown to bind various azole drugs tightly, and selected azoles were also shown to be effective in treatment of TB in a mouse model [8,10,11]. However, drug targeting against FprA may prove a challenge given its structural similarity to host AdR and other reductases, and since coenzyme analogue inhibitors are very unlikely to prove specific to FprA. Antitubercular pro-drugs such as isoniazid and ethionamide have nicotinamide-like moieties and are activated (by the catalase-peroxidase KatG and the Baeyer-Villiger monooxygenase EtaA) to reactive forms that have at least one common nicotinamide coenzyme-dependent target; the NADH-dependent enoyl-acyl carrier protein

reductase InhA [29,30]. While it is conceivable that other NAD(P)H-dependent Mtb enzymes are targeted by these drugs, there is no proof to date that FprA is one such target.

In conclusion, characterization of FprA R199A, R200A and R199A/R200A mutants highlights the importance of these phylogenetically conserved residues in controlling the thermodynamic properties and reactivity of FprA. Arg199 and Arg200 are clearly critical residues controlling the affinity of binding of NADPH (and hence stabilization of the SQ form of FprA leading to its greater stability to auto-oxidation), in controlling coenzyme selectivity (NADPH *versus* NADH) and in modulating FAD potential (likely through long-range interactions). Moreover, Arg199 and Arg200 have important functions in positioning of the coenzyme backbone and nicotinamide ring to optimise reactivity and to facilitate efficient electron transfer between coenzyme and cofactor in both oxidative and reductive directions. Future work on this enzyme will involve detailing its cellular interactions with ferredoxin partner(s) in Mtb P450 redox systems.

## ACKNOWLEDGEMENTS

This work was funded by grant awards to the authors from the UK Biotechnology and Biological Sciences Research Council (BBS/B/06288) and from the EU (6$^{th}$ Framework Programme Integrated Project NM4TB). AWM thanks the Royal Society for the award of a Leverhulme Trust Senior Research Fellowship. DL is a Royal Society University Research Fellow. NSS is a BBSRC Professorial Research Fellow.

## REFERENCES

[1] Laurenzi, M., Ginsberg, A. and Spigelman, M. (2007). Challenges associated with current and future TB treatment. Infect. Disord. Drug Targets. **7**, 105-119.

[2] Ginsberg, A.M. and Spigelman, M. (2007). Challenges in tuberculosis drug research and development. Nat. Med. **13**, 290-294.

[3] Saint-Joanis, B., Souchon, H., Wilming, M., Johnsson, K., Alzari, P.M. and Cole, S.T. (1999). Use of site-directed mutagenesis to probe the structure, function and isoniazid activation of the catalase/peroxidase, KatG, from *Mycobacterium tuberculosis*. Biochem. J. **338**, 753-760.

[4] World Health Organization report on "Global tuberculosis control – surveillance, planning, financing; at http://www.who.int/tb/publications/global_report/2007/en/index.html.

[5] Cole, S.T., Brosch, R., Parkhill, J., Garnier, T., Churcher, C, Harris, D., Gordon, S.V., Eiglmeier, K., Gas, S., Barry, C.E. 3rd, Tekaia, F., Badcock, K., Basham, D., Brown, D., Chillingworth, T., Connor, R., Davies, R., Devlin, K., Feltwell, T., Gentles, S., Hamlin, N., Holroyd, S., Hornsby, T., Jagels, K., Krogh, A., McLean, J., Moule, S., Murphy, L., Oliver, K, Osborne, J., Quail, M.A., Rajandream, M.A., Rogers, J., Rutter, S., Seeger, K., Skelton, J., Squares, R., Squares, S., Sulston, J.E., Taylor, K., Whitehead, S. and Barrell, B.G. (1998) Deciphering the biology of *Mycobacterium tuberculosis* from the complete genome sequence. Nature **393**, 537-544.

[6] McLean, K.J., Clift, D., Lewis, D.G., Sabri, M., Balding, P.R., Sutcliffe, M.J., Leys, D. and Munro, A.W. (2006). The preponderance of P450s in the *Mycobacterium tuberculosis* genome. Trends Microbiol. **14**, 220-228.

[7] Podust, L.M., Poulos, T.L. and Waterman, M.R. (2001) Crystal structure of cytochrome P450 14α-sterol demethylase (CYP51) from *Mycobacterium tuberculosis* in complex with azole inhibitors. Proc. Natl. Acad. Sci. USA **98**, 3068-3073.

[8] McLean, K.J., Warman, A.J., Seward, H.E., Marshall, K.R., Girvan, H.M., Cheesman, M.R., Waterman, M.R. and Munro, A.W. (2006). Biophysical characterization of the sterol demethylase P450 from *Mycobacterium tuberculosis*, its cognate ferredoxin, and their interactions. Biochemistry **45**, 8427-8443.

[9] Odds, F.C., Brown, A.J. and Gow, N.A. (2003). Antifungal agents: mechanisms of action. Trends Microbiol. **11**, 272-279.

[10] McLean, K.J.,Marshall, K.R., Richmond, A., Hunter, I.S., Fowler, K., Kieser, T., Gurcha, S.S., Besra, G.S. and Munro, A.W. (2002). Azole antifungals are potent inhibitors of cytochrome P450 mono-oxygenases and bacterial growth in mycobacteria and streptomycetes. Microbiology **148**, 2937-2949.

[11] Ahmad, Z., Sharma, S. and Khuller, G.K. (2006). Azole antifungals as novel chemotherapeutic agents against murine tuberculosis. FEMS Microbiol. Lett. **261**, 181-186.

[12] Munro, A.W., Girvan, H.M. and McLean, K.J. (2007) Variations on a (t)heme: novel mechanisms, redox partners and catalytic functions in the cytochrome P450 superfamily. Nat. Prod. Rep. **24**, 585-609.

[13] Bellamine, A., Mangla, A.T., Nes, W.D. and Waterman, M.R. (1999) Characterization and catalytic properties of the sterol 14alpha-demethylase from *Mycobacterium tuberculosis*. Proc. Natl. Acad. Sci. USA **96**, 8937-8942.

[14] Bossi, R.T., Aliverti, A., Raimondi, D., Fischer, F., Zanetti, G., Ferrari, D., Tahallah, N., Maier, C.S., Heck, A.J., Rizzi, M. and Mattevi, A. (2002) A covalent modification of $NADP^+$ revealed by the atomic resolution structure of FprA, a *Mycobacterium tuberculosis* oxidoreductase. Biochemistry **41**, 8807-8818.

[15] McLean, K.J., Scrutton, N.S. and Munro, A.W. (2003) Kinetic, spectroscopic and thermodynamic characterization of the *Mycobacterium tuberculosis* adrenodoxin reductase homologue FprA. Biochem. J. **372**, 317-327.

[16] Ziegler, G.A., Vonrhein, C., Hanukoglu, I. and Schulz, G.E. (1999) The structure of adrenodoxin reductase of mitochondrial P450 systems: electron transfer for steroid biosynthesis. J. Mol. Biol. **289**, 981-990.

[17] Muller, J.J., Lapko, A., Bourenkov, G., Ruckpaul, K. and Heinemann, U. (2001) Adrenodoxin reductase-adrenodoxin complex structure suggests electron transfer path in steroid biosynthesis. J. Biol. Chem. **276**, 2786-2789.

[18] Leys, D., Mowat, C.G., McLean, K.J., Richmond, A., Chapman, S.K., Walkinshaw, M.D. and Munro, A.W. (2003) Atomic structure of *Mycobacterium tuberculosis* CYP121 to 1.06 Å reveals novel features of cytochrome P450. J. Biol. Chem. **278**, 5141-5147.
[19] Neeli, R., Sabri, M., McLean, K.J., Dunford, A.J., Scrutton, N.S., Leys, D. and Munro, A.W. (2008). Tryptophan 359 regulates flavin thermodynamics and coenzyme selectivity in *Mycobacterium tuberculosis* FprA. Biochem. J. **411**, 563-570.
[20] Sambrook, J., Fritsch, E. F., and Maniatis, T. (1989) Molecular Cloning: A Laboratory Manual, 2nd Ed., Cold Spring Harbor Laboratory Press, Cold Spring Harbor, NY.
[21] Roitel, O., Scrutton, N.S., and Munro, A.W. (2003) Electron transfer in flavocytochrome P450 BM3: Kinetics of flavin reduction, the role of cysteine 999, and relationships with mammalian cytochrome P450 reductase. Biochemistry **42**, 10809-10821.
[22] Munro A.W., Noble, M.A., Robledo, L., Daff, S.N., and Chapman, S.K. (2001) Determination of the redox properties of human NADPH-cytochrome P450 reductase. Biochemistry **40**, 1956-1963.
[23] Dutton, P.L. (1978) Redox potentiometry: determination of midpoint potentials of oxidation-reduction components of biological electron-transfer systems. Methods Enzymol. **54**, 411-435.
[24] Daff, S.N., Chapman, S.K., Turner, K.L., Holt, R.A., Govindaraj, S., Poulos, T.L., and Munro, A.W. (1997) Redox control of the catalytic cycle of flavocytochrome P-450 BM3. Biochemistry **36**, 13816-13823.
[25] Lawson, R.J., von Wachenfeldt, C., Haq, I., Perkins, J. and Munro, A.W. (2004) Expression and characterization of the two flavodoxin proteins of *Bacillus subtilis*, YkuN and YkuP: biophysical properties and interactions with cytochrome P450 BioI. Biochemistry **43**, 12390-12409.
[26] Fischer, F., Raimondi, D., Aliverti, A. and Zanetti, G. (2002) *Mycobacterium tuberculosis* FprA, a novel bacterial NADPH-ferredoxin reductase. Eur. J. Biochem. **269**, 3005-3013.
[27] McLean, K.J., Dunford, A.J., Sabri, M., Neeli, R., Girvan, H.M., Balding, P.R., Leys, D., Seward, H.E., Marshall, K.R. and Munro, A.W. (2006). CYP121, CYP51 and associated redox systems in *Mycobacterium tuberculosis*: towards deconvoluting enzymology of P450 systems in a human pathogen. Biochem. Soc. Trans. **34**, 1178-1182.
[28] Dunford, A.J., McLean, K.J., Sabri, M., Seward, H.E., Heyes, D.J., Scrutton, N.S. and Munro, A.W. (2007). Rapid heme iron reduction by laser photoexcitation of *Mycobacterium tuberculosis* CYP121 and CYP51B1. Analysis of CO complexation reactions and reversibility of the P450/P420 equilibrium. J. Biol. Chem. **282**, 24816-24824.
[29] Baulard, A.R., Betts, J.C., Engohang,-Ndong, J., Quan, S., McAdam, R.A., Brennan, P.J., Locht,. C. and Besra, G.S. (2000). Activation of the pro-drug ethionamide is regulated in mycobacteria. J. Biol. Chem. **275**, 28326-28331.
[30] Vannelli, T.A., Dykman, A. and Ortiz de Montellano. P.R. (2002). The antituberculosis drug ethionamide is activated by a flavoprotein monooxygenase. J. Biol. Chem. **277**, 12824-12829.
[31] Neeli, R., Roitel, O., Scrutton, N.S. and Munro, A.W. (2005) Switching pyridine nucleotide specificity in P450 BM3: mechanistic analysis of the W1046H and W1046A enzymes. J. Biol. Chem. **280**, 17634-17644.

# TABLES

**Table 1. Steady-state kinetic parameters for WT FprA and the R199A, R200A and R199A/R200A mutants.** Steady-state parameters were determined as described in the *Experimental* section. Reaction rate data were determined using an extinction coefficient of $\Delta\varepsilon_{420}$ = 1020 $M^{-1}$ $cm^{-1}$ for ferricyanide reduction, and rate *versus* NAD(P)H concentration data were fitted using a hyperbolic function to derive the reported $k_{cat}$ and $K_m$ parameters. Values in parentheses in the final column indicate the fold change in the catalytic efficiency (with NADH relative to NADPH) for the relevant mutant compared to WT FprA, based on the ratio of the specificity constants with NADH and NADPH as electron donors. For the double mutant only, data were fitted to a substrate inhibition equation (Equation 1) to produce the $k_{cat}$ and $K_m$ values detailed. The corresponding $K_i$ value determined for NADH with the double mutant (and using the same function) was 250 ± 52 μM.

| FprA Protein | $k_{cat}$ ($min^{-1}$) | | | $K_m$ (μM) | | | $k_{cat}/K_m$ ($\mu M^{-1}$ $min^{-1}$) | | | $\frac{k_{cat}/K_m \text{ NADH}}{k_{cat}/K_m \text{ NADPH}}$ |
|---|---|---|---|---|---|---|---|---|---|---|
| | $Fe(CN)_6^{3-}$ | NADPH | NADH | $Fe(CN)_6^{3-}$ | NADPH | NADH | $Fe(CN)_6^{3-}$ | NADPH | NADH | |
| WT | 2010 ± 100 | 2070 ± 100 | 2720 ± 90 | 5.9 ± 1.2 | 3.8 ± 0.5 | 427 ± 42 | 341 ± 86 | 545 ± 97 | 6.4 ± 0.8 | 0.012± 0.004 (1) |
| R199A | 2880 ± 140 | 2880 ± 130 | 2960 ± 70 | 4.0 ± 0.9 | 24.1 ± 4.1 | 158 ± 18 | 719 ± 19 | 120 ± 26 | 18.7 ± 2.6 | 0.16 ± 0.06 (13.3) |
| R200A | 2450 ± 70 | 2580 ± 70 | 2730 ± 60 | 6.7 ± 1.3 | 12.3 ± 1.5 | 80.0 ± 10.9 | 366 ± 86 | 210 ± 31 | 34.1 ± 5.4 | 0.16 ± 0.05 (13.3) |
| R199/200A | 254 ± 13 | 302 ± 23 | 830 ± 38 | 14.4 ± 3.1 | 16.7 ± 4.7 | 18.8 ± 5.3 | 17.6 ± 4.1 | 18.1 ± 6.5 | 44.1 ± 14.5 | 2.4 ± 1.7 (200) |

**Table 2. Kinetic parameters for NAD(P)H-dependent reduction of FAD in WT and mutant FprA enzymes.** Data reporting on FAD reduction in WT and R199A, R200A and R199A/R200A FprA mutants were collected using stopped-flow absorption spectroscopy as described in the *Experimental* section. The values for the limiting rate of electron transfer from coenzyme to FAD ($k_{lim}$) and the apparent dissociation constant for the coenzyme ($K_d$) are derived from hyperbolic fits of observed FAD reduction rates *versus* the relevant coenzyme concentrations. In the case of WT FprA, there was no apparent dependence of the observed NADPH-dependent FAD reduction rate in the *pseudo* first order regime, and thus a value for $K_d$ was not determinable (ND). *For WT FprA, the value reported for $k_{lim}$ is the rate observed at near-saturating concentrations of NADPH.

| FprA Protein | $k_{lim}$ ($s^{-1}$) | | $K_d$ (μM) | | $k_{lim}/K_d$ ($\mu M^{-1} s^{-1}$) | | $\frac{k_{lim}/K_d \text{ (NADH)}}{k_{lim}/K_d \text{ (NADPH)}}$ |
|---|---|---|---|---|---|---|---|
| | NADPH | NADH | NADPH | NADH | NADPH | NADH | |
| WT | *20.0 ± 2.0 | 25.4 ± 0.7 | ND | 42.9 ± 4.6 | ND | 0.59 ± 0.08 | ND |
| R199A | 29.0 ±1.4 | 25.7 ± 0.9 | 28.3± 4.3 | 54.0 ± 9.4 | 1.0 ± 0.2 | 0.47 ± 0.10 | 0.48 ± 0.20 |
| R200A | 27.5 ± 0.5 | 24.9 ± 1.0 | 42.6 ± 5.8 | 32.1 ± 7.2 | 0.65 ± 0.10 | 0.78 ± 0.21 | 1.2 ± 0.5 |
| R199/200A | 22.2 ± 0.5 | 26.7 ± 1.4 | 88.6 ± 7.7 | 64.4 ± 13.9 | 0.25 ± 0.03 | 0.41 ± 0.11 | 1.6 ± 0.6 |

**Table 3. Aerobic oxidation rates for WT and mutant forms of FprA.** The rate of reoxidation of WT and mutant FprA enzymes with oxygen as the electron acceptor was determined using enzymes (20 μM) stoichiometrically reduced with coenzyme, and as described in the *Experimental* section [15]. An exponential function was fitted to the data to generate the rate constants detailed.

| | Oxidation rate ($min^{-1}$) | |
|---|---|---|
| **FprA enzyme** | **NADPH** | **NADH** |
| **Wild-type** | 0.043 ± 0.004 | 1.26 ± 0.06 |
| **R199A** | 0.77 ± 0.02 | 0.88 ± 0.03 |
| **R200A** | 0.96 ± 0.02 | 1.70 ± 0.10 |
| **R199A/R200A** | 1.13 ± 0.05 | 1.50 ± 0.12 |

**Table 4. FAD midpoint reduction potentials for WT and mutant forms of FprA.** The midpoint reduction potential ($E_m$) for the FAD cofactor in WT, R199A, R200A and R199A/R200A FprA enzymes was determined by spectroelectrochemical titration, as described in the *Experimental* section [8,30]. Potentials are reported relative to the standard hydrogen electrode (SHE).

| | FAD Reduction potential (mV *versus* SHE) | |
|---|---|---|
| **FprA enzyme** | **Ligand-free** | **$H_4$NADP-bound** |
| **Wild-type** | -230 ± 12 | -235 ± 5 |
| **R199A** | -165 ± 4 | -174 ± 5 |
| **R200A** | -192 ± 4 | -233 ± 4 |
| **R199A/R200A** | -172 ± 4 | -202 ± 6 |

# FIGURES

**Figure 1. Structure and coenzyme binding site of *Mtb* FprA.** Figure 1A shows the atomic structure of the crystallographic dimer of Mtb FprA with alpha helices in blue, beta sheets in green and random coil sections depicted in pink. The FAD cofactor is in yellow spacefill in both monomers. Figure 1B shows a magnification of the NADP(H) binding region of FprA. The $NADP^+$ coenzyme, FAD cofactor and relevant amino acids (Arg199, Arg200 and Trp359) are shown as coloured sticks. The nicotinamide end of the $NADP^+$ molecule approaches the isoalloxazine ring of the FAD, with the side chain of Trp359 in close proximity. The side chains of Arg199 and Arg200 make stabilizing electrostatic interactions with the 2'-phosphate group of the $NADP^+$. Alpha helices are in cyan and beta sheet regions in magenta. Structural images were prepared using Pymol (DeLano Scientific) and the coordinates of the $NADP^+$-bound form of FprA (PDB code 1LQT) [14].

**Figure 2. Electronic absorption spectra for WT and mutant FprA enzymes.** Absorption spectra are shown for WT FprA (44 μM, panel A), R200A FprA (42 μM, panel B) and R199A/R200A FprA (42 μM, panel C). In each case, oxidised protein is shown as a thin black line, NADPH-reduced as a thick line, NADH-reduced as a dotted line and dithionite-reduced as a dashed line. Spectra for the R199A mutant are essentially identical to those for the R199A/R200A double mutant. There is no significant accumulation of blue SQ in NADPH-reduced R199A or R199A/R200A mutants, and the amount formed in the R200A mutant is substantially less than in the WT FprA.

**Figure 3. Kinetics of NAD(P)H-dependent FAD reduction in FprA mutants**. Data were collected using stopped-flow absorption spectroscopy, as described in the *Experimental* section. The figure shows a plot of observed FAD reduction rate *versus* NADPH concentration for the FprA R200A mutant. Equation 2 was fitted to the data to provide parameters for the limiting rate constant for FAD reduction ($27.5 \pm 0.5\ s^{-1}$) and for the apparent $K_d$ for the coenzyme ($42.6 \pm 5.8$ μM). A similar data set for the R199A/R200A mutant is presented as Figure S2 in the *Supplementary Data*.

**Figure 4. Photodiode array analysis of coenzyme-dependent reduction and oxidation of FprA mutants.** Panel A shows selected UV-visible spectra collected during the stopped-flow NADPH-dependent reduction of the FprA R199A mutant. Spectra shown were collected between 0.00384 s (first spectrum shown) and 1.023 s (final spectrum shown) following the mixing event. Panel B shows the comparable spectral set for NADPH-dependent reduction of the R200A mutant (spectra shown collected between 0.00128 and at 4.594 s). Panel C shows spectra collected during the reaction of fully reduced R199A mutant with $NADP^+$ (spectra shown collected between 0.01152 and 5.024 s). Panel D shows spectra collected during the reaction of fully reduced R200A mutant with $NADP^+$ (spectra shown collected between 0.00128 and 0.04992 s, negligible further change was observed up to 2 s following the initiation of the reaction). In all cases, the final amount of enzyme present in the mixture was 20 μM, and coenzyme was in 10-fold molar excess (200 μM).

**Figure 5. Potentiometric analysis of the FprA R200A mutant.** Panel A shows the optical changes accompanying reductive potentiometric titration of the ligand-free R200A mutant (77 μM). Arrows indicate direction of absorption change (at the oxidised flavin absorption peaks) as the potential becomes more negative. Spectra shown cover the range from -16 mV to -362 mV (*versus* the standard hydrogen electrode, SHE). Panel B shows an overlay of the data fits (using a 2-electron Nernst function, as described previously [8,25,31]) for the ligand-free R200A mutant (closed squares) and for the $H_4$NADP-bound form (open circles). The fits were computed using $A_{452}$ data (at the oxidised FAD maximum), and then data converted to "FAD oxidised (%)" using the parameters generated and in order to show both data sets on exactly the same scale. $H_4$NADP-binding results in a 41 mV decrease in reduction potential from -192 mV to -233 mV.

Biochemical Journal Immediate Publication. Published on 03 Sep 2008 as manuscript BJ20080466



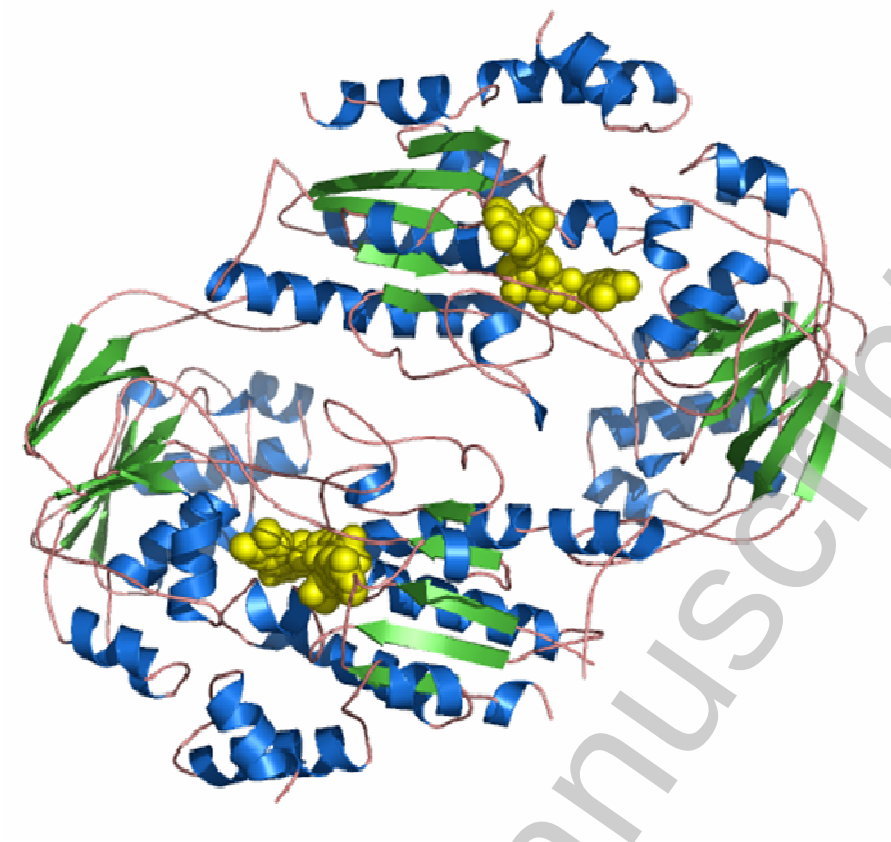

**Figure 1A**

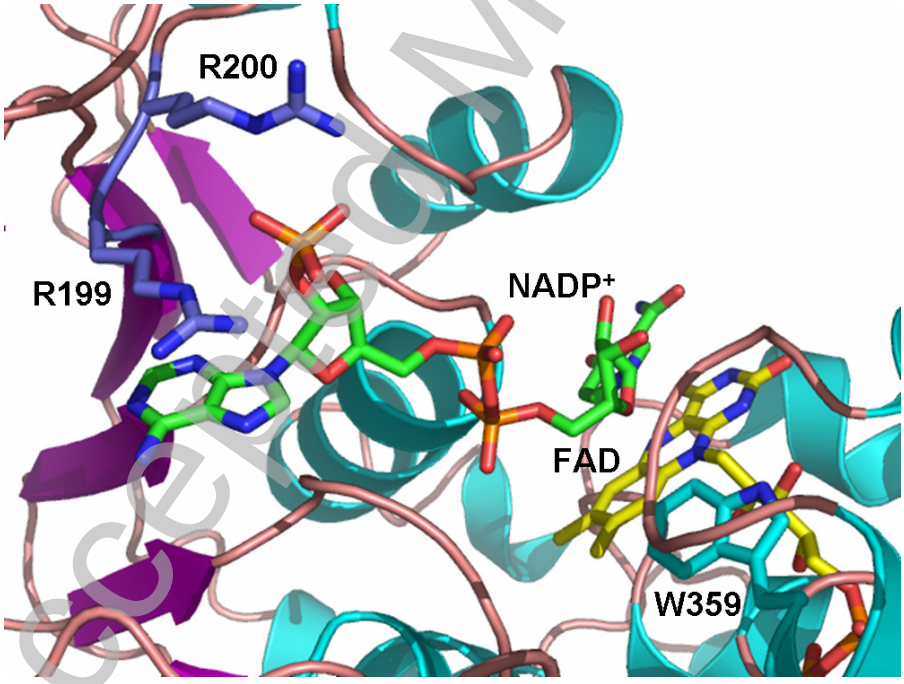


**Figure 1B**

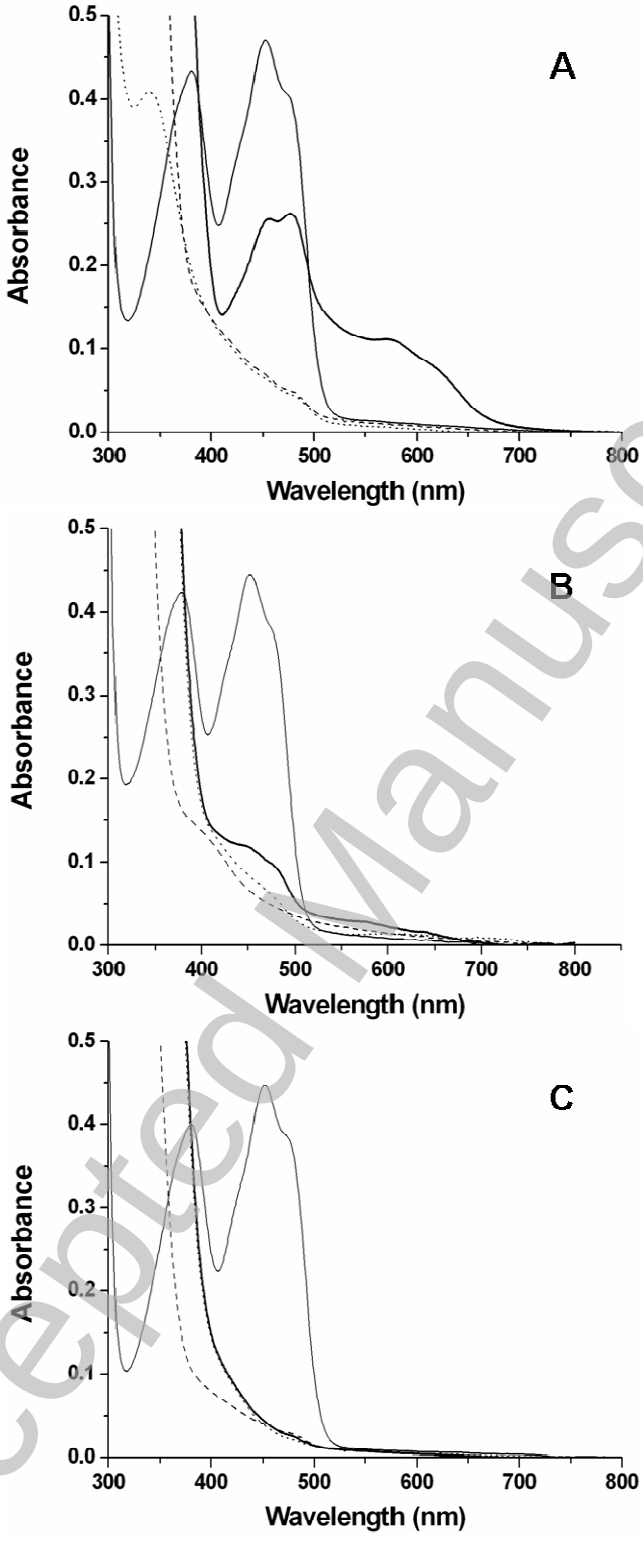


**Figure 2**

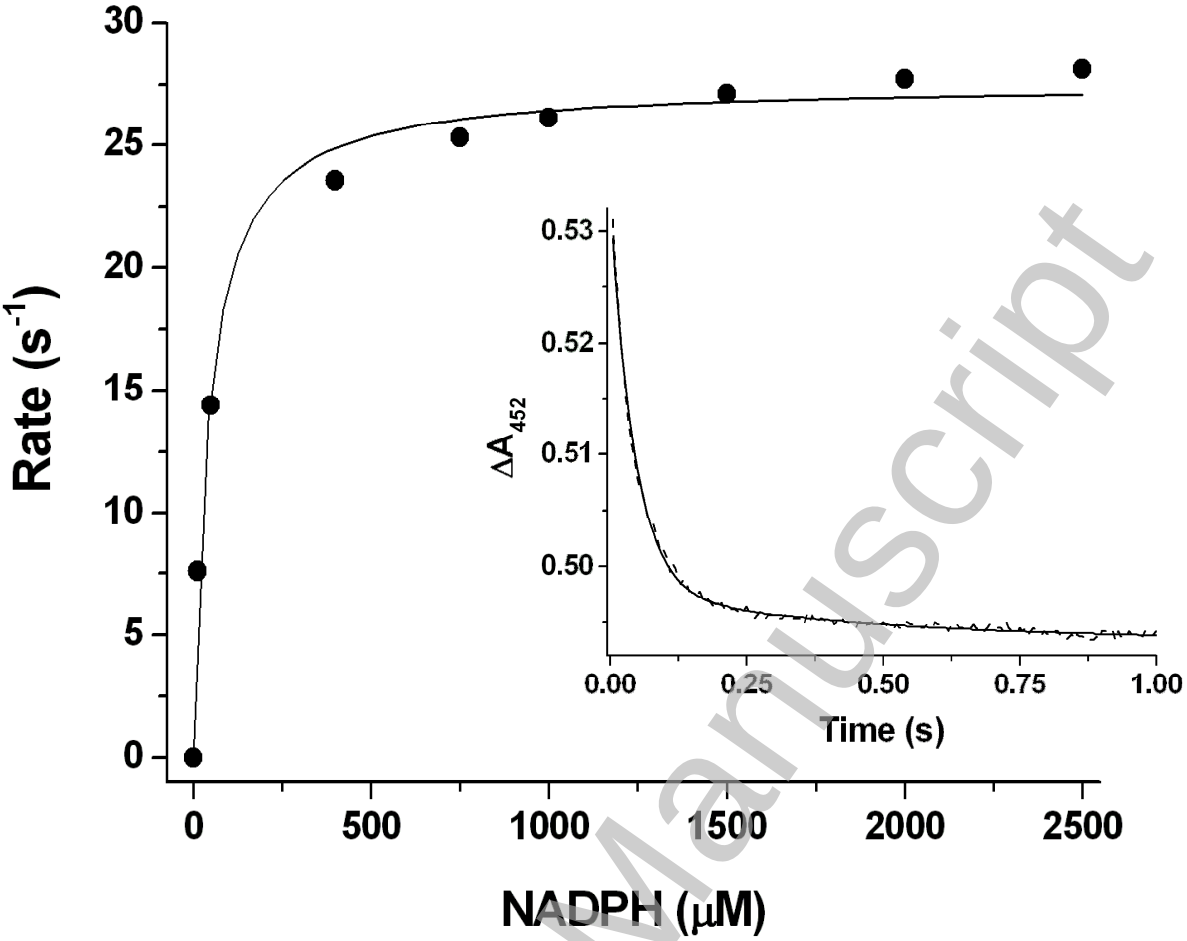


**Figure 3**

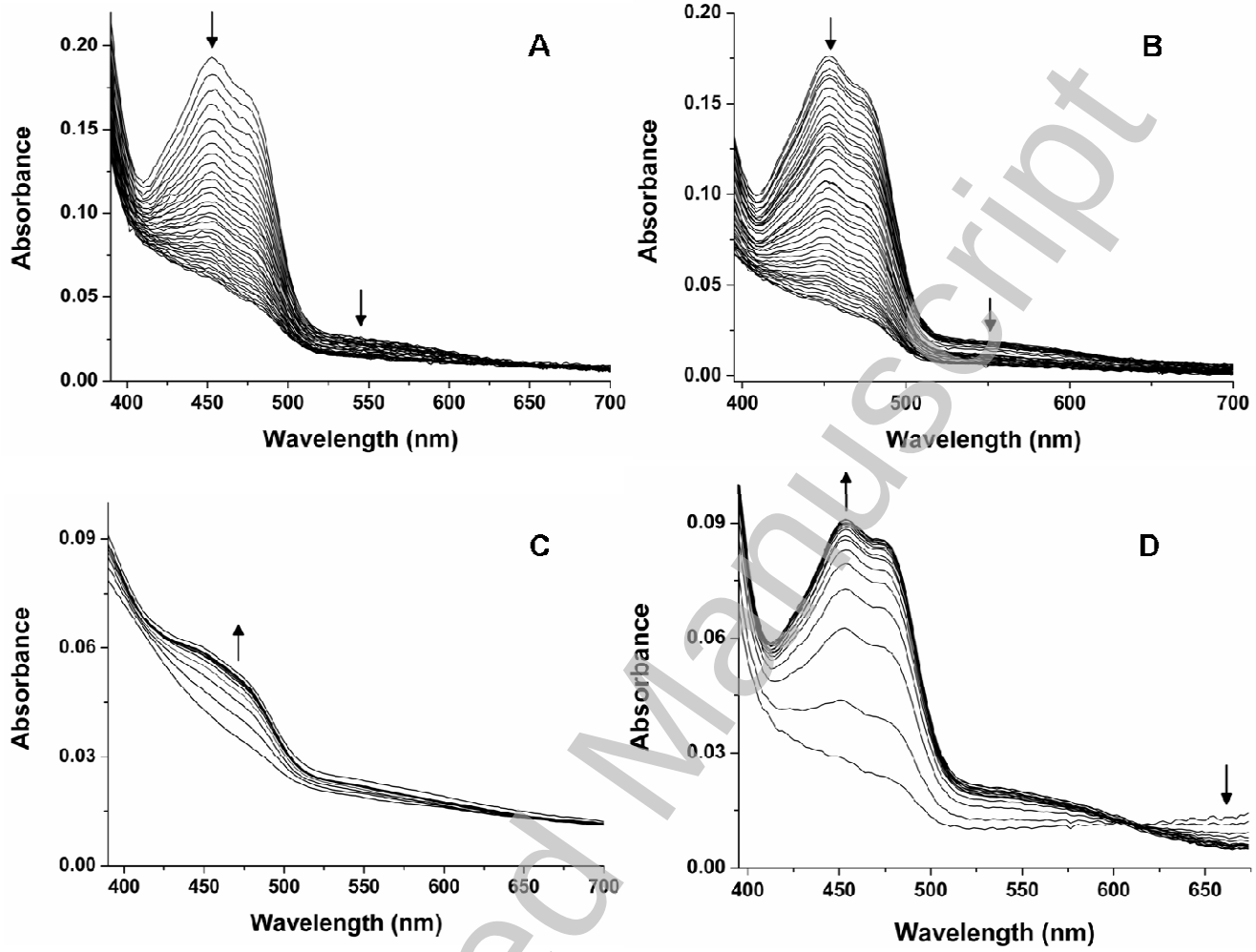


**Figure 4**

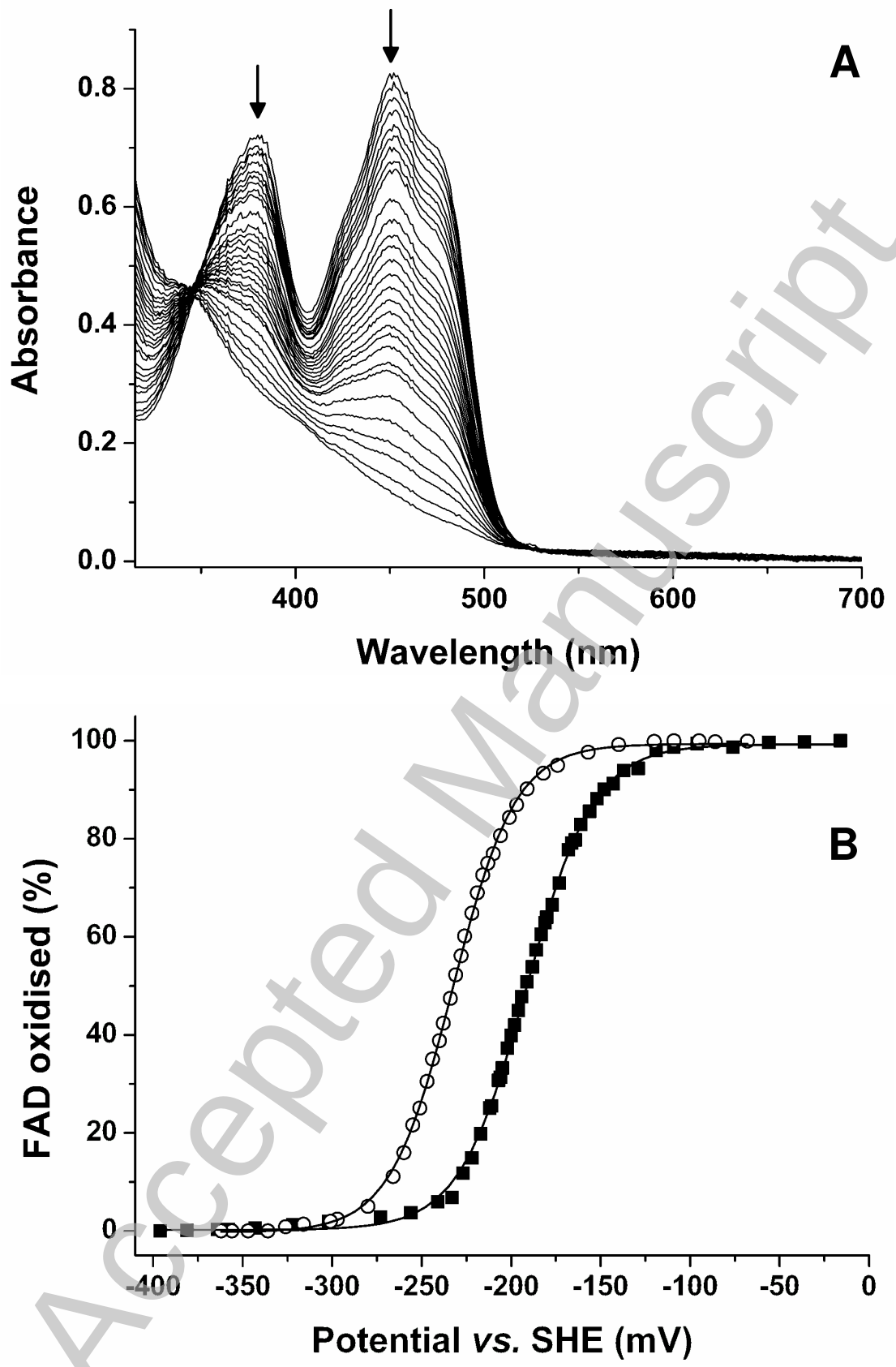


**Figure 5**